The Formation and Maintenance of Density Fronts on the U.S. Southeastern Continental Shelf during Winter

LIE-YAUW OEY

Skidaway Institute of Oceanography, Savannah, GA 31416

(Manuscript received 6 June 1985, in final form 8 October 1985)

ABSTRACT

Density fronts on the U.S. southeastern continental shelf, during winter, are formed by (i) breakdown of the shelf-break front by Gulf Stream meanders or strong southward winds or both, (ii) shoreward intrusion of upper Gulf Stream warm water by persistent southward winds, and (iii) mixing of this warm water with continental shelf water cooled by cycles of cold air outbreaks. A cross-shelf and depth, time-dependent numerical model, which includes a model Gulf Stream and vertical mixing calculated according to a second-moment, turbulence closure submodel, was used to study physical processes involved in the formation and maintenance of continental shelf fronts. Model results using somewhat idealized atmospheric forcings suggest that three or more winter storms are required to establish fronts on the midshelf. Otherwise, the front is situated just inshore of, and is sometimes indistinguishable from, the shelf-break front. Once formed, the front is maintained by southward winds, which transport warm water converging at the front and prevent frontal weakening by balancing seaward advection of cooler water at the foot of the front with downward turbulent diffusion of warmer water. Mean along-front flow is about 5 cm s^{-1} northward, opposing the wind, and should contribute to the persistent northward flow observed on the continental shelf during winter. Model results agree qualitatively with available hydrographic data.

One- and two-dimensional model simulations were performed for a two and a half month period during winter 1983/84 when wind, air and water temperature data were available at a nearshore ocean station. Simulated circulation and density structures confirm the idealized model run. Calculated temperature variations agree fairly well with observations, except for a discrepancy during a warm period from 1–18 December 1983, when incident solar radiation (minus longwave back radiation), neglected in the model, was significant.

1. Introduction

The formation of temperature contrasts across continental shelf waters resulting from forcings by winter cold air outbreaks (CAO) was apparently first described by Nowlin and Parker (1974) for coastal waters in the northwestern Gulf of Mexico. Strong wind stress and dry, cold air which usually accompany a CAO result in a large loss of heat from the comparatively warm sea. Shelf waters, which may be stratified before the winter season, become vertically well-mixed, either throughout the entire water column, or down to a depth of about 100 m where the local water depth is deeper. Cross-shelf temperature contrasts form because the nearshore, shallower waters cool more rapidly than adjacent, deeper offshore waters. During the transient period immediately following a CAO, regions of strong horizontal thermal contrasts or fronts are often formed (Huh et al., 1978), due either to local topographic changes in depth, or to divergence/convergence induced by the strong winds. Such thermal fronts become truly dynamic fronts when the σ_t distribution also has strong horizontal gradients. Such density fronts are evident in the data given by Nowlin and Parker (1974, their Figs. 7 and 11), for example. Huh et al. (1978) and Garwood et al. (1981, Figs. 1 and 7) show sea surface temperature (SST) fronts from satellite imageries which, assuming that the waters were well-mixed and that salinity values were fairly uniform horizontally, would also indicate density fronts. Circulation around such density fronts involves strong (~10 cm s^{-1}) along-front flow, surface convergences, frontal upwellings and downwellings.

Density fronts can be quite persistent throughout the entire winter season. An example of persistency is the shelf/slope front described by Garwood et al. (1981). In this case, cold, nearshore shelf water was separated from warmer slope and open ocean water and thermal contrasts conformed almost precisely to the 20 m bathymetry around the Little and Great Bahama Banks. The formation and maintenance of such shelf/slope fronts depend on rather abrupt changes in water depth between shelf and slope regions, in addition to the necessary atmospheric cooling events. Over a gently sloping shelf, on the other hand, fronts persist for only a few days after a major CAO. Such is the case for fronts described on the Gulf of Mexico shelf by Nowlin and Parker (1974). Their Fig. 7, for example, shows that surface σ_t prior to a CAO was broad, diffuse and gently varying in cross-shore distance. It appears then, if fronts

formed over a gently sloping shelf region are to persist throughout the winter season, some persistent mechanisms like wind-induced convergence/divergence must operate after the fronts are formed by cycles of winter storms. Temperature fronts frequently observed on the continental shelf in the South Atlantic Bight during winter provide perhaps one example of such frontal maintenance over a gently sloping shelf. This study addresses the dynamics of formation and maintenance of these continental shelf fronts.

In section 2, observations from winter hydrographic surveys and current meter records are given to show the existence of continental shelf fronts which are quite separate from, but closely related to, the "western wall" of the Gulf Stream front. Section 3 describes winter atmospheric conditions and, section 4 proposes a hypothetical working model for continental shelf frontal formation. To understand the dynamics and thermodynamics of continental shelf fronts, a numerical modeling study is utilized to show how these fronts are formed and maintained from combined actions of cycles of CAO, wind forcings and intrusions of upper Gulf Stream water. A description of the model and its inputs is given in section 5. Section 6 discusses model response to a set of idealized, but representative, wintertime atmospheric forcings. In section 7, model response to observed atmospheric forcings for winter 1983/84 are discussed, and simulated and observed water temperatures at a nearshore station on the 17 m isobath are compared. Finally, section 8 concludes the paper and also gives recommendations for future modeling studies of wintertime continental shelf/Gulf Stream dynamics and thermodynamics.

2. Observational evidence of temperature fronts on continental shelf

a. *Hydrographies*

Hydrographic data from the U.S. southeastern continental shelf during the winter season are limited. Examples of existing data, collected along cross-isobath/depth sections, with shoreward origins at St. Simons and Savannah, Georgia, are shown in Figs. 1 and 2. These show crowding of isotherms at about the mid-shelf region and variations in both time and cross-shelf spatial extent (Fig. 1 and 14–16°C isotherms in Fig. 2). Shoreward intrusions of upper Gulf Stream water (Figs. 1c and 2), and "shelf break fronts" which cannot be distinguished from the "western wall" of the Gulf Stream are also evident. Hydrographic data from summer to early autumn show strongly stratified upper Gulf Stream water with isopycnals extending horizontally over the shelf break and onto the continental shelf (e.g., see Fig. 1 in Atkinson, 1977). Wintertime temperature contrasts between upper Gulf Stream and continental shelf waters and intense mixing produced by convective overturning and strong winds combine with changes in bottom topography across the shelf break to form the shelf break front (cf. Garwood et al., 1981). Intrusions of upper Gulf Stream water onto the shelf occur as this front breaks down and warm water spills shoreward mixing with cold continental shelf water to form a secondary front on the continental shelf. The frontal structure bounded by the 17° and 21°C isotherms in Fig. 2 shows such shoreward movement of the shelf break front. In addition to wind-generated water movements, I believe these processes of wind forcing, continental shelf cooling, Gulf Stream intrusion and the subsequent shoreward movement of warm water are important in the study of the dynamics and thermodynamics of shelf circulation during winter.

b. *Current meter data*

The breakdown of shelf break fronts can be due either to Gulf Stream meanders or strong wind-induced shoreward movement of the upper mixed layer of the Gulf Stream or both. Intrusion processes during winter have been described by Lee (1978). Current meters deployed along the 75 m isobath (the shelf break) between 30° and 32°N latitudes, from about mid-December 1976 through mid-April 1977, gave negative values for the cross correlation $\langle u'T' \rangle$ between the [40-hour low passed (HLP)] cross-isobath velocity fluctuation u' (positive offshore) and (40-HLP) temperature fluctuation, T', at 17 m depth, and positive values at 72 m depth. Negative $\langle u'T' \rangle$ at the top meter location implies an onshore transport of warm water from the upper Gulf Stream. Positive $\langle u'T' \rangle$ at the bottom meter location suggests either (i) onshore transport of cold anomalies or (ii) offshore transport of warm water to the cooler, bottom slope water region. Process (i) is consistent with transient upwellings while (ii) is consistent with a cross-slope and depth, two-dimensional picture in which, following an initial onshore intrusion and subsequent mixing with outer shelf water mass, upper warm Gulf Stream water is returned to the deeper, somewhat colder slope water. In either case, $\langle u'T' \rangle$ at top meter locations were 10 to 20 times larger in absolute magnitudes than the lower meter readings and some onshore intrusion must have taken place at the shelfbreak.

Monthly wind climatologies from Weber and Blanton (1980) and Kantha et al. (1981) show winds from the north-northwest during winter. Lee (1978) found that mean currents on the shelf region along the 30 and 40 m isobaths were northward against the mean wind stress direction, consistent with Bumpus' (1973) wintertime drifter data. Thus, a northward force strong enough to overcome mean wind forcing must be exerted on the water column. Perhaps density fronts across the continental shelf region contribute significantly to such northward forcing.

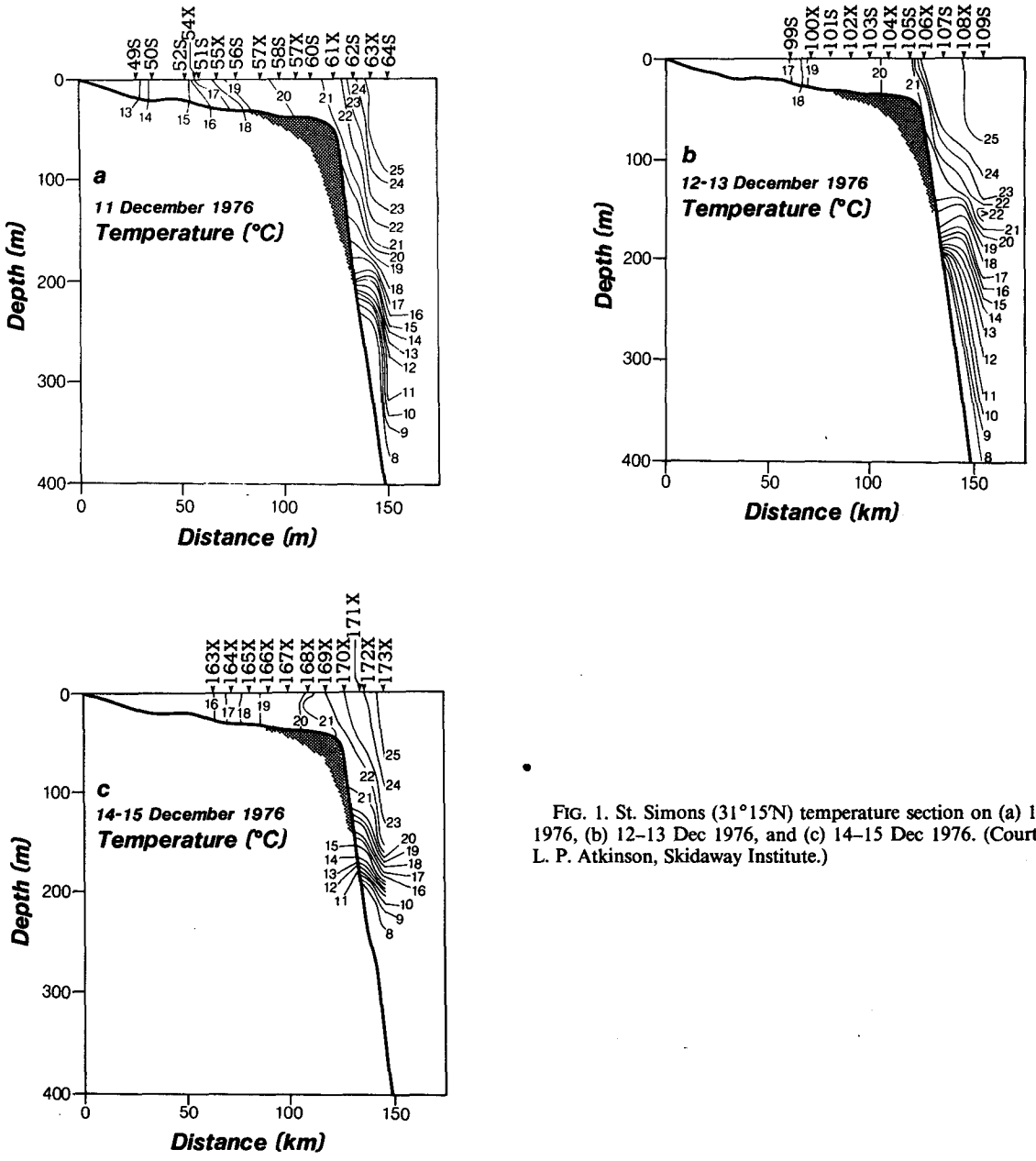

FIG. 1. St. Simons (31°15'N) temperature section on (a) 11 Dec 1976, (b) 12–13 Dec 1976, and (c) 14–15 Dec 1976. (Courtesy of L. P. Atkinson, Skidaway Institute.)

3. Atmospheric forcings

Winter atmospheric conditions off the U.S. southeastern continental shelf consist of cyclone passages at periods of 3–10 days. These cyclones, which introduce strong winds and cold, relatively dry air over the continental shelf, produce intense vertical mixing of the upper water layer and latent and sensible heat losses of up to 600 W m^{-2} (see section 7, Fig. 15). Figure 3 shows time series data of daily averaged air temperature, relative humidity and wind speed and direction taken from NOAA local climatological data at the Sa-

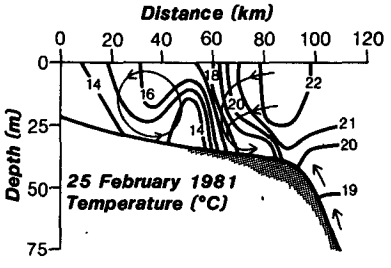

FIG. 2. Savannah (32°N) temperature section on 25 Feb 1981. Courtesy of J. A. Yoder, Skidaway Institute. Circulation pattern suggested by model results are superimposed.

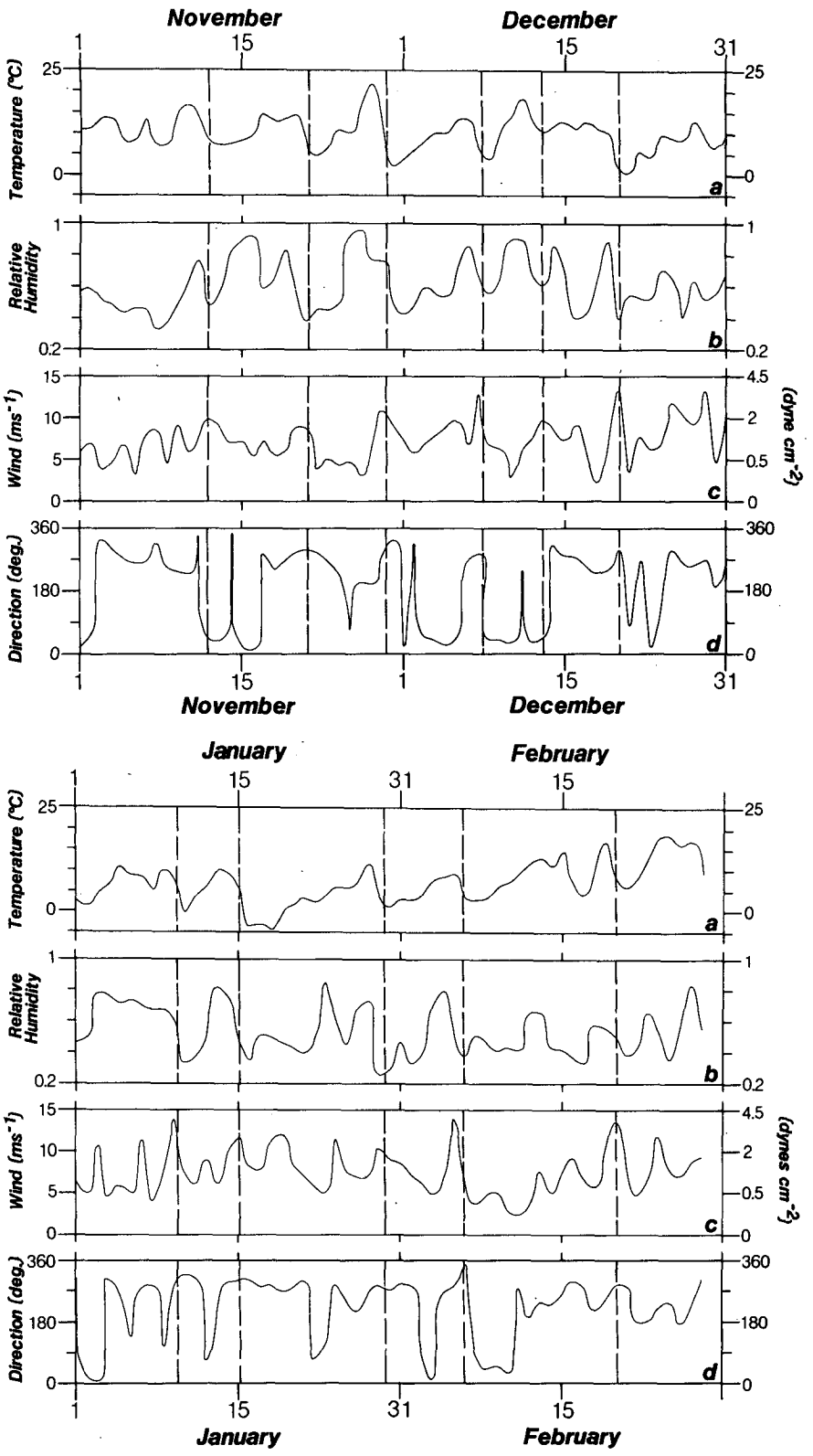

FIG. 3. Air temperature (°C), relative humidity and wind speed (m s^{-1}) and direction (from where wind blows, degrees clockwise from true north), measured at Savannah airport for the period Nov 1976 through Feb 1977. Vertical dashed lines indicate times of cyclone passage.

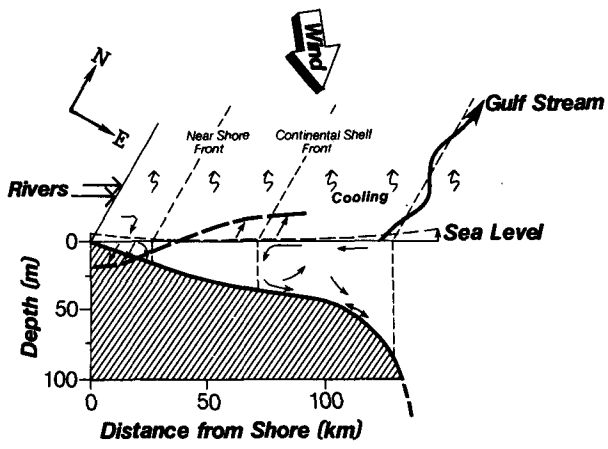

FIG. 4. A hypothetical model of the wintertime mean circulation in the U.S. southeastern continental shelf region.

vannah airport from November 1976 through February 1977. Periodic cyclones, which crossed the area, are marked in the figure. During these periods, average wind speeds reached 10 m s^{-1} with direction generally from the northwest, air temperature dropped by as much as 6–10°C and relative humidity was low (0.3–0.5).

4. A hypothetical model

The formation and maintenance of continental shelf fronts are shown schematically in Fig. 4. Repeated cycles of winter cooling from CAOs and associated intense southward winds result in large heat and evaporative mass losses from the ocean. While nearshore water cools faster than that at the outer shelf, the shelf bottom topography is too gentle and the mixed layer depth which results from intense wind mixing and convective overturning is too deep (~100 m) to form a thermal frontal zone by the process described by Garwood et al. (1981). However, thermal frontal zones can still form following a major CAO (Huh et al., 1978). These are positioned close to the shore and over time are dissipated and diffused seaward by wind and tidal mixings. In addition to winter cooling, a continuous supply of warm water at the shelf break by intrusion from the northward meandering Gulf Stream is required to form a front on the continental shelf.

In Fig. 4 the nearshore frontal zone has also been sketched in. Such nearshore fronts, during autumn, are formed by river discharge of low salinity water (Blanton, 1981) and presumably disappear with the onset of winter when evaporation and cooling increase nearshore water density. If this occurs, the sea level slope in Fig. 4 may need to be modified. Mean along-shelf currents at mid- to outer-shelf locations are northward with magnitudes ranging from 2–17 cm s^{-1} (Bumpus, 1973; Lee, 1978). Close to shore, frictional dynamics dominate and southward mean wind and sea level setup at the coast are presumably sufficient to drive a southward flow (see also Blanton, 1981).

5. A mathematical model

A two-dimensional, cross-shelf and depth time-dependent numerical model (Fig. 5) was chosen to study the physical processes hypothesized for the formation and maintenance of continental shelf fronts. The model is clearly somewhat idealized: alongshore homogeneity; smoothly varying bottom topography with a constant depth of 1500 m in the open ocean; a Gulf Stream system maintained by specifying open ocean σ_t (rather than specifying northward transport); no fresh water discharge at the coast and no tidal forcing. In spite of these assumptions, I believe that the model describes first-order dynamics: vertical mixing by wind and convective overturning with subsequent formation of upper ocean mixed layer; cooling of ocean water by CAOs with faster cooling of shelf water than slope and open ocean waters; shoreward movements of upper Gulf

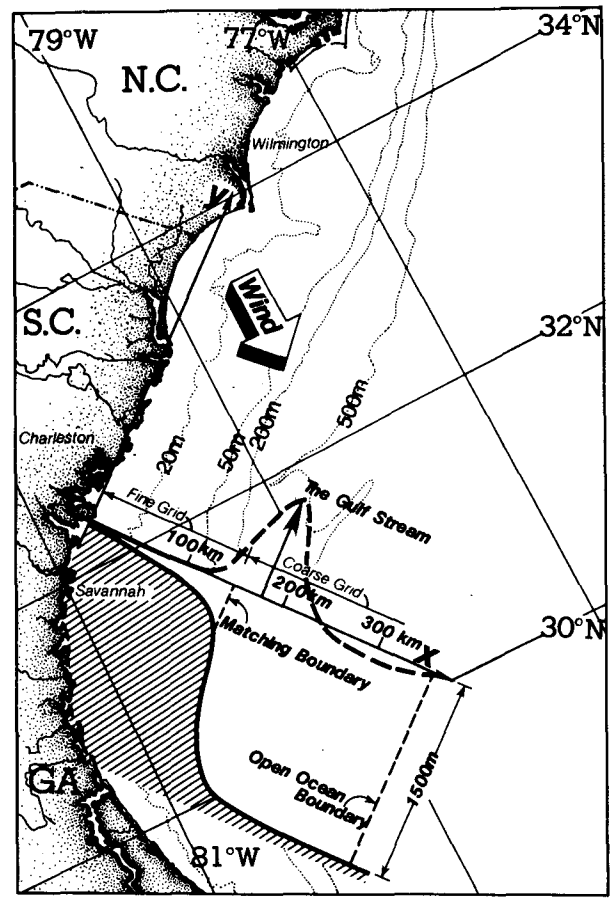

FIG. 5. A sketch of the numerical model domain and its geographical relation to the U.S. southeastern continental shelf region.

Stream warm water induced by the wintertime southward component of wind stress following breakdown of the shelf-break front; and subsequent flushing of the continental shelf water mass. The assumption of along-shelf homogeneity excludes important Gulf Stream meander processes (Brooks and Bane, 1983) because along-shelf wave propagation is not supported by the model. Breakdowns of the shelf break front can only be simulated, therefore, by specifying cross-shelf flow perturbations. This is done by specifying the wintertime southward component wind stress.

a. Model equations

The governing equations are obtained, as a special case of our three-dimensional circulation and mixing model for coastal waters (Oey et al., 1985a), by setting all y-derivatives equal to zero.

$$U_x + W_z = 0 \tag{1}$$

$$U_t + (U^2)_x + (UW)_z - fV = -P_x/\rho_0 - (\overline{wu})_z \tag{2}$$

$$V_t + (UV)_x + (VW)_z + fU = -(\overline{vw})_z \tag{3}$$

$$\rho g = -P_z \tag{4}$$

$$E_t + (UE)_x + (WE)_z = -(\overline{we})_z \tag{5}$$

$$\rho = \rho(T, S), \tag{6}$$

where x, y, z are respective offshore (southeastward), alongshore (northeastward) and upward vertical coordinate axes; the origin is at the mean sea level; t is time; $U + u$, $V + v$ and $W + w$ are instantaneous velocities in the x, y and z directions, respectively, $E + e$ denote instantaneous temperature or salinity where U, V, W and E denote the ensemble means and u, v, w and e the corresponding fluctuating quantities; $\overline{uw}$, $\overline{vw}$ and $\overline{we}$ are turbulent Reynolds fluxes defined by

$$(-\overline{uw}, -\overline{vw}) \equiv K_M(U_z, V_z), \quad -\overline{we} \equiv K_H E_z, \tag{7}$$

where K_M is the turbulent mixing coefficient for momentum and K_H the turbulent diffusion coefficient for temperature and salinity; f is the Coriolis parameter; ρ is the mean density and ρ_0 is a reference density; g is the acceleration due to gravity and P is the pressure. I have made the hydrostatic assumption in (4) and Boussinesq assumption. The equation of state, (6), is taken from Fofonoff (1962).

Here K_M and K_H are calculated according to Mellor and Yamada's (1982) level 2.5 turbulence model wherein,

$$K_M = S_M l q, \quad K_H = S_H l q, \tag{8}$$

l is the turbulence length scale and $q^2/2$ is the turbulence kinetic energy. They are calculated from turbulence transport equations of the form

$$DF/Dt = (\text{diffusion of } F) + (\text{shear and buoyancy productions of } F) + (\text{dissipation of } F), \tag{9}$$

where F denotes either $q^2/2$ or $q^2 l$. The S_M and S_H are stability factors which depend on q, l and vertical velocity and buoyancy gradients. The turbulence closure model has been developed and refined over a decade and has been used successfully in a number of geophysical fluid problems (Mellor and Yamada, 1982; Hassid and Galperin, 1983, 1984; Dickey and van Leer, 1984; Oey et al., 1985a,b,c). Martin (1985) tested the model by simulating observed mixed layers and SST at two ocean stations and found fairly good results without adjusting the model's constants (mean percentage errors for SST for the two stations were 2% and 7%). While there is certainly room for improvement, I feel that the model is sufficient for the present purpose.

b. Boundary conditions

Boundary conditions at the free surface, $z = \eta(x, t)$, are:

$$\left.\begin{aligned} K_M(U_z, V_z) &= (\tau_{0x}, \tau_{0y}) \\ K_H(T_z, S_z) &= (\dot{T}, \dot{S}) \\ q^2 &= \text{constant}|\tau_0| \\ q^2 l &= 0 \\ W &= U\eta_x + \eta_t \end{aligned}\right\}, \tag{10}$$

where $\tau_0 = (\tau_{0x}, \tau_{0y})$ is the wind stress vector, $\dot{T} = -Q/(\rho_0 C_{pw})$ and $\dot{S} = S(x, z = 0, t)E_v/\rho_0$, where Q is the total upward heat flux in W m^{-2}, C_{pw} is the specific heat for water ($\approx$4000 J kg^{-1} K^{-1}, from Gill, 1982, Table A3.1) and E_v is the rate of evaporation in kg m^{-2} s^{-1}.

At the bottom, the boundary conditions for T, S, q^2 and $q^2 l$ are similar to those at the surface with $\dot{T} = \dot{S} = 0$ and bottom friction replaces τ_0. For W, we have

$$W = -UH_x \quad \text{at} \quad z = -H(x), \tag{11}$$

and for U and V, the computed solutions are matched with the turbulence law of the wall which extends the computed U and V into the viscous or roughness sublayer where the no-slip condition at the ocean floor is satisfied. Thus,

$$(U, V) \sim [(-\overline{wu}, -\overline{wv})/ku_*] \ln[(H + z)/z_0] \quad \text{as} \quad z \to -H, \tag{12}$$

where u_* is the bottom friction velocity, $k = 0.40$ is von Karman's constant and z_0 is the roughness height. For the results in this paper, $z_0 = 1.0$ cm.

At the coast, $x = 0$, $U = 0$. At the open ocean boundary, $x \approx 300$ km, "standard" (e.g., see Oey et al., 1985a)

open ocean conditions are applied: T and S are specified during inflow and a radiation condition is used during outflow. Results at the continental shelf break and shelf region are not sensitive to conditions at the (sufficiently far) open ocean end.

Details of the numerical algorithm, which includes split external/internal mode, sigma coordinates, implicit tridiagonal solver etc., can be found in Blumberg and Mellor (1983). A new feature of the model is the fine grid–coarse grid system used, in which a grid change is made at approximately the 350 m isobath (Fig. 5). This feature is outlined in the Appendix; it can be easily implemented in many finite-difference numerical models. The coarse grid used in the open ocean region allows one to use a larger Δt constrained by larger gravity phase speeds there. For the present study, $\Delta x_{\text{fine}} = 2$ km and $\Delta x_{\text{coarse}} = 6$ km. I have also performed model experiments with $(\Delta x_{\text{fine}}, \Delta x_{\text{coarse}}) = (1 \text{ km}, 4 \text{ km})$ and (2 km, 10 km) with little changes in the final results were performed. The finest mesh test calculation was for 18 days only because it became very expensive. Typical runs [with (2 km, 6 km) grid] on SKIO's minicomputer PRIME 550 took approximately one hour for three days of simulation.

c. *Model initialization and spin-up run*

The model was initialized to approximate, as close as possible, observed autumn hydrography: vertically mixed continental shelf region with $T = 20°C$, $S = 32‰$ near the coast and $S = 35‰$ at the shelf break. The slope and deep ocean waters are stratified with $T = 20°$ to 26°C and $S = 35‰$ to 36.2‰ increasing seaward at the base of a mixed layer depth of about 50 m, and $T = 18°$ to 8°C decreasing seaward, S = constant = 35‰ near the bottom.

The model was spun-up from these initial conditions with zero wind stress and zero surface heat and mass fluxes until the kinetic energies, averaged separately over the continental shelf (coast to 100 m isobath) and the open ocean regions, became asymptotically steady. The shelf region settled to an equilibrium state in about 10 days whereas the open ocean region required 20 days to reach equilibrium. The calculation was continued for an additional 10 days beyond the 20-day spin-up time (cf. Blumberg and Mellor, 1983). Figure 6 shows field variables at the end of the 30-day spin-up calculation. Maximum Gulf Stream velocity after this spin-up run is about 1.5 m s^{-1} near the surface, and −0.05 m s^{-1} near the bottom over the 500 m isobath. This equilibrium field will be used as the initial condition for the following model calculation.

6. Model response to idealized wintertime atmospheric forcings

I have chosen somewhat idealized atmospheric forcings which should, nevertheless, portray wintertime conditions with periods of CAO (Fig. 7). Air temperature starts at 20°C, fairly typical of late autumn, and decreases by 6.5°C in 12 hours while a southward wind increases from 0 to about 14 m s^{-1}. These values are kept constant for five days after which wind is decreased to zero and air temperature increased to a value 2°C lower than at the start of the cooling event. This quiescent period persists for 12 days before another storm arrives and the process continues. To minimize inertial

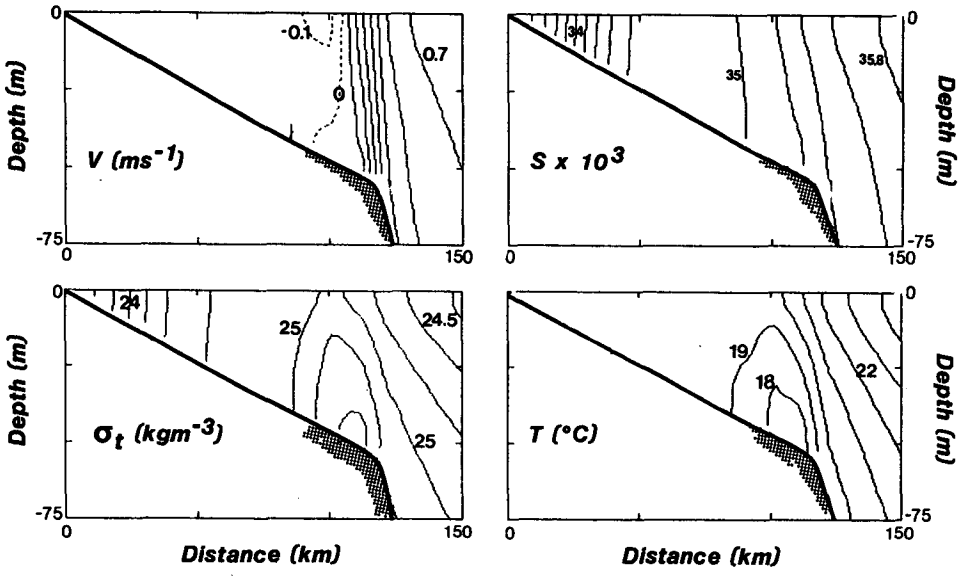

FIG. 6. Field variables at the end of 30-days spinup model run: contours of alongshelf velocity (m s^{-1}) density (σ_t, kg m^{-3}), salinity ($S \times 10^3$) and temperature (°C).

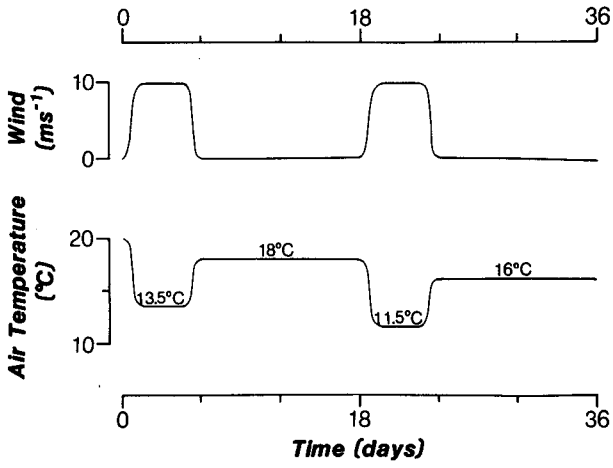

FIG. 7. Atmospheric forcings used in model study of response of continental shelf water to cycles of wintertime storms. The speed is for southeastward (model offshore) and southwestward (model negative alongshore) wind. Maximum resultant wind is therefore southward at about 14 m s^{-1}.

oscillations, all forcings are smoothed in time for about one inertial period so that they do not attain their maximum values until time $\approx$ 20 h (Fig. 7). Model results are averaged over one-inertial period before being written on tapes. These procedures do not, however, completely remove inertial oscillations. Therefore, a rather long 12-day dissipation period has been allowed before examining the "true" mean fields. This long quiescent period (long compared with an observed period of about five days between cyclone passages) will not impact the physical mechanisms proposed in section 4 on the formation of continental shelf fronts. The model's southward wind stress averaged over the 18 day period is 0.85 dyn cm^{-2}, approximately equal to monthly mean wind stress during winter given by Kantha et al. (1981).

The following bulk aerodynamic formulae are used to compute kinematic wind stress τ_0 and upward sensible heat flux Q_s:

$$\tau_0 = (\rho_a/\rho_0)C_D|\mathbf{u}_a|\mathbf{u}_a \tag{13a}$$

$$Q_s = \rho_a C_{pa} C_H |\mathbf{u}_a|(T_0 - T_a) \tag{13b}$$

where ρ_a and C_{pa} are air density and specific heat respectively, $\mathbf{u}_a$ and T_a the wind vector and air temperature at 10 m level, T_0 the sea surface temperature equated to the surface grid point in the model, and C_D and C_H are eddy exchange coefficients taken to be equal to 2×10^{-3} and 1.7×10^{-3}, respectively (see Kantha et al., 1981). In section 7, where the model will be forced with observed atmospheric forcings, the rate of evaporation E_v will be computed from a bulk aerodynamic formula

$$E_v = \rho_a C_H |\mathbf{u}_a|(q_0 - q_a). \tag{14a}$$

The upward latent heat flux is given by

$$Q_l = L_v E_v, \tag{14b}$$

where q_0 and q_a are specific humidities at the sea surface under saturated condition and at the 10 m level, respectively, $L_v \approx 2.5 \times 10^6$ J kg^{-1} is the latent heat of vaporization of water, and the eddy exchange coefficient for evaporation flux has been equated to C_H. For the present idealized forcing case, q_a is not known and the empirical Bowen ratio

$$B = Q_s/Q_l, \tag{15}$$

given as a function of air–sea temperature difference in Roll (1965, p. 253–254), was used to compute Q_l.

The total upward heat flux is

$$Q = Q_s + Q_l, \tag{16}$$

and therefore a balance is assumed between longwave back radiation heat flux Q_B (from ocean to atmosphere) and incident solar radiation Q_I. This obviously oversimplifies the real situation especially that Huh et al. (1984) showed how significantly Q_I can vary during a CAO. This rapid transient forcing should have little impact on the first-order dynamics of the circulation studied here.

a. Model results: The shelf-break front

Figure 8 shows velocity and density fields at t = 5 days, near the end of the first forcing event. Recall that wind is from due north and model wind stress therefore

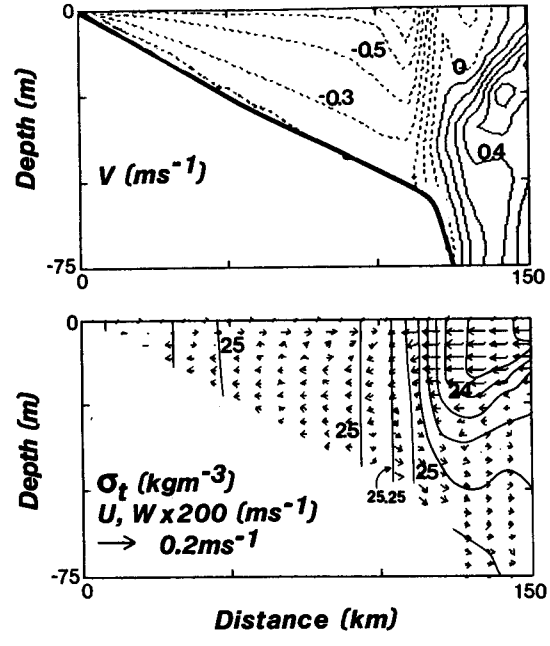

FIG. 8. Computed velocity (cross-shore U and alongshore V) and density fields at t = 5 days, near the end of the first atmospheric forcing event. Velocity arrows are plotted at every third grid point.

has both an offshore (positive x) and a southwest alongshore (negative y) component. Flow over the continental shelf quickly (~18 hours) settles to frictional equilibrium condition with large southwestward alongshore velocity of the order of 0.4 m s^{-1}, in geostrophic balance with the cross-shelf sea level gradient. An offshore wind stress component produces offshore velocity near the surface, and coastal constraint dictates a compensating onshore return flow in the thicker bottom layer, both of a few cm s^{-1}. Over the shelf break and slope regions, direct influence of the coast and bottom is small, and the model southward wind stress produces a westward Ekman transport in the upper mixed layer (~25 m) of the model Gulf Stream. This produces both northwestward onshore and southwestward alongshore flow components. The onshore flow brings warm water onto the shelf and, together with the offshore surface layer flow in the shelf region, forms a convergent zone just inshore of the shelf break. The downwelling water below the surface convergence accelerates seaward. For this first forcing event, shelf water cooling is insignificant and the front over the shelf break is formed by onshore flow of warm water and differences in mixed layer depths between the shallow shelf and deep slope regions.

Figure 9 shows velocity and density fields at t = 6.5 days, 12 hours after the end of the first forcing event. Alongshore velocity over the continental shelf region has decreased to about ⅓ of its magnitude at t = 5 days. Cross-shelf sea level gradients decrease in magnitude and, being no longer balanced wholly by the alongshore flow, produce a net offshore (barotropic) transport of water. Cross-shelf velocity over the continental shelf region reverses sign with near bottom flow now accelerating seaward while near surface flow is directed shoreward, being no longer driven by an offshore wind. Beyond the shelf break, coastal constraint on cross-shelf sea level gradient is negligible. The pool of warm water in the upper 20 m of the model Gulf Stream continues to flow shoreward and, being opposed by a now weakened offshore pressure gradient on the continental shelf, intrudes about 15 km further onto the shelf. The front is sheared, so to speak, by oppositely directed near-surface and near-bottom flows, and a local two-layer system with anticlockwise circulation is formed. The front is qualitatively similar to the shelf-break front described by Wang (1984) for the Middle Atlantic Bight, with downward motion at the head of, and upward motion behind, the front. The difference is that, in the present case, less dense water is over the slope region and there is downwelling over the outer-shelf which accelerates seaward. One can qualitatively compare model response with observed hydrographic data shown in Fig. 1. From 10–13 December 1976, the wind was from the northeast increasing in speed from about 3 m s^{-1} to 10 m s^{-1}; air temperature dropped about 8°C and relative humidity dropped from 0.8 to 0.6 (Fig. 3). Figure 1b shows isotherms closely packed at the shelf break. Wind speed decreased to about 7 m s^{-1} on the 15th and there was a shoreward movement of upper water over the shelf break, as indicated by the 21°C isotherm in Fig. 1c. In reality, one cannot ignore other Gulf Stream intrusion processes, and the effect of wind forcing must be assessed in comparison with these processes.

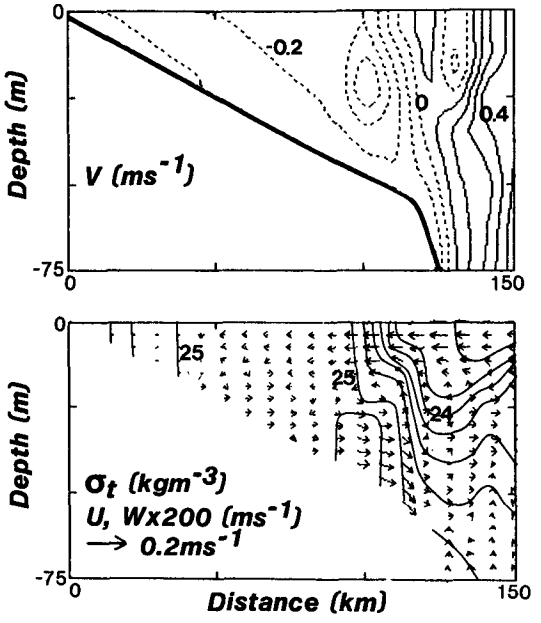

FIG. 9. As in Fig. 8, but for density fields at t = 6.5 days, one-half day after the end of the first atmospheric forcing event.

b. *Model results: Fronts on the continental shelf*

At the beginning of the winter season, continental shelf water is not sufficiently cooled and only a shelf-break front is formed. A series of winter storms is required to establish a frontal zone on the continental shelf. Figure 10 shows the mean velocity, turbulence diffusivity, temperature and density fields at t = 36 days, twelve days after the second forcing event had stopped and any (leaked) inertial oscillations had decayed. A front centered around the 40 m isobath is formed by further onshore movement of the shelf-break front described previously. Temperature contrasts are due to warm (~23°C) Gulf Stream water on the seaward side and cool (~18°C) shelf water on the shoreward side of the front. This temperature front is similar to observed frontal structures bounded by the 17° and 21°C isotherms shown in Fig. 2. These observations were made following a winter cyclone with CAO and strong southward wind which lasted for about a week. Model results suggest an intrusion of warm Gulf Stream water in the upper three-quarters of the water column, sinking at the head (18°C isotherm) of the front, a

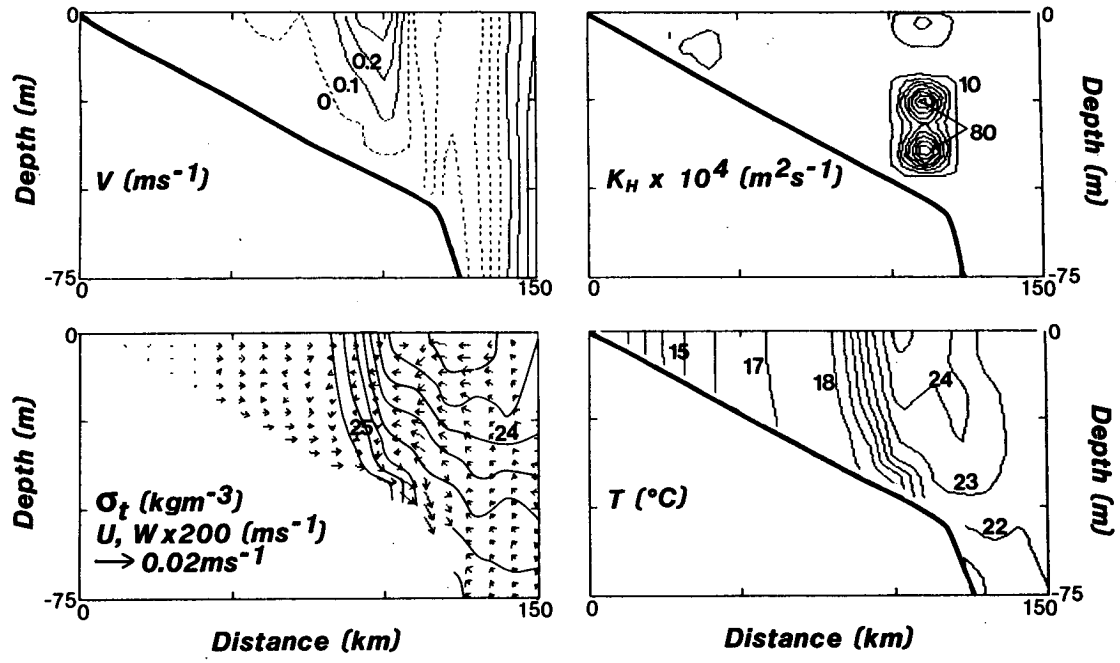

FIG. 10. Computed mean velocity, turbulence diffusivity, density and temperature fields at $t = 36$ days, 12 days after the second atmospheric forcing event has stopped. Arrows plotted as in Fig. 8.

near-bottom seaward flow at the foot of the front and an upwelling flow in the continental slope region. Computed turbulence diffusivity is greatest behind the front in the lower half of the water column, reaching maximum values of about 80 cm^2 s^{-1}. The large mixing is due to convective overturning caused by more intense recirculating flow in this region.

Along-front velocities are about 20 cm s^{-1}, in the positive y direction, and are therefore directed against the mean wind during winter. The southwestward alongshore velocity found at the shelf break and slope is unrealistic and stems from the way the Gulf Stream was modeled as a "passive" front maintained by a cross-front density gradient. The upper 100 m or so of this front is weakened by the applied southward wind stress because of (i) depletion of initial northeastward momentum and (ii) decreased cross-front dynamic height gradient by inclined isopycnals due to shoreward transport of warm water. A more realistic model would be three-dimensional in which one can specify northward transport. In the following, the slope and open ocean region will be treated, therefore, as a pool of warm water and model results concentrated on the continental shelf region.

Figures 11 and 12 show a series of density and cross-plane velocity fields which illustrate how a third forcing event leads to break-up of the front at the 40 m isobath (Figs. 11a–b), formation of a new front farther shoreward at the 30 m isobath (Figs. 11b–c) and final formation of a single, more diffused front across the continental shelf (Fig. 12). The break-up process is due to a farther shoreward movement of the upper, shallow front (Figs. 11a–b). This shallow front breaks away from its parent front as it moves inshore to shallower shelf regions where wind mixing is strong enough to overcome stabilizing buoyancy forces, and a second, surface-to-bottom frontal zone is formed (Fig. 11c). The double front structure thus formed is similar to observed temperature contours shown in Fig. 2. Examination of local climatology at the Savannah airport reveals similarities in forcing conditions. Strong southward winds, with speeds reaching over 10 m s^{-1}, occurred on 14–16, 20–21 and 23–24 February. Air temperature decreased from 17° to 12°C from 19 through 25 February. Wind speed decreased to 5 m s^{-1} on 25 February and remained southward when the temperature section was taken. Thus, observation approximates a sudden stop of southward wind stress. Model results (Fig. 11c) suggest two recirculating regions with upward and downward water movements between the two fronts. These circulation patterns are sketched in Fig. 2. Note the "dome" of denser bottom water just inshore of the shelf break ($x \approx 700$ km) formed by seaward downwelling of cold mixed Gulf Stream and continental shelf waters, rather than by direct upwelling from the slope region, as one might perhaps infer from the density field alone (Fig. 11c).

Final relaxation (Fig. 12) consists of frontal dispersion induced primarily by near-bottom, downslope accelerating flow. Two recirculating cells remain with the stronger one centered on the outer shelf region. The cross-front velocity component is of the order of 1 cm

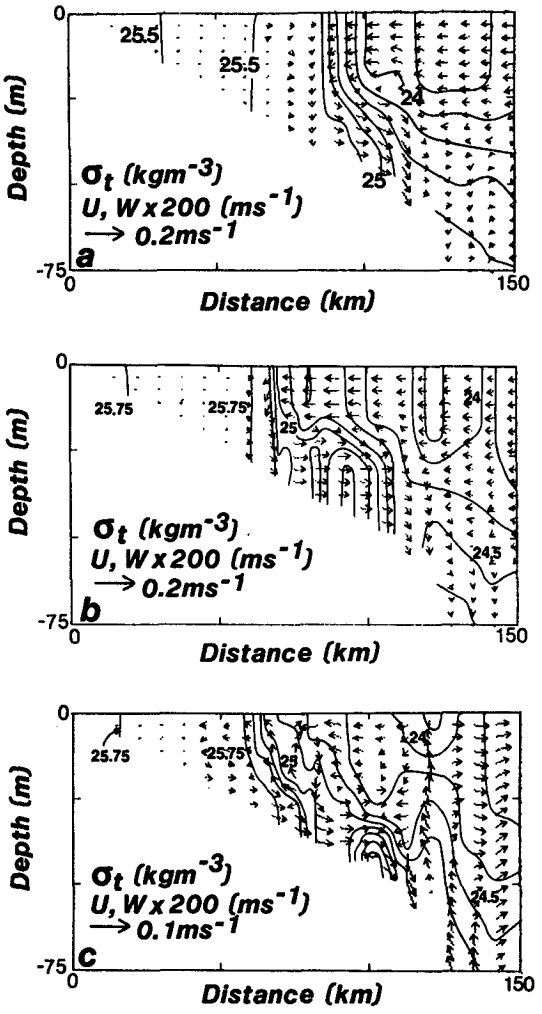

FIG. 11. Computed cross-plane velocity and density fields at (a) t = 37 days, (b) t = 41 days and (c) t = 43 days. (a) and (b) correspond respectively to 1-day and 5-days after the start of the third atmospheric forcing event and (c) corresponds to 1-day after the forcing has stopped. Arrows plotted as in Fig. 8.

s^{-1}. The along-front velocity component is of the order of 10 cm s^{-1} directed northeastward at the surface layer and there is a thin layer near the bottom where the flow is southwestward.

7. Model simulation for winter 1983/84

To demonstrate how continental shelf fronts are formed by physical processes discussed in previous sections, a description of model results obtained using observed atmospheric forcings is provided here. Wind and air temperature observations are available from 5 November 1983 through 20 January 1984 (Fig. 13) at the Savannah Navigational Light Tower (SNLT) located at approximately the 17 m isobath about 20 km seaward of Savannah. Because dew-point temperature was not measured at the tower, values from the Savannah airport local climatological data record were used. Figure 13 shows a series of CAOs with strong northwesterlies and northeasterlies. Major events occurred from 18 December 1983 through 1 January 1984 and again from 11 through 20 January. The extreme case occurred on 25 December 1983 when air temperature dropped below −8°C. Corresponding relative humidities are also shown in Fig. 13, and are converted into specific humidities for use in Eq. (14) to calculate latent heat flux. Water temperatures at 4 m below the surface were also measured at SNLT and will be compared with model results.

Model initial conditions are similar to those shown in Fig. 6, except that nearshore water temperature was set to correspond to SNLT measured value of 21°C on 5 November. Model results (not shown) indicate that a shelf-break front was formed fairly early in the simulation following intrusion-favorable southwestward winds 5–10 November. The front was occasionally displaced seaward by northeastward winds but temperature contrast across the front strengthened as the shelf water cooled. With the series of southwestward winds beginning on 17 December, intrusion of warm Gulf Stream water occurred. As an example, Fig. 14 shows the alongshore velocity, turbulence diffusivity, temperature and density and cross-frontal circulation fields for 20 January. Density structure shows a front situated just inshore of the shelf break, similar to Fig. 9. Intense vertical mixing is primarily produced by

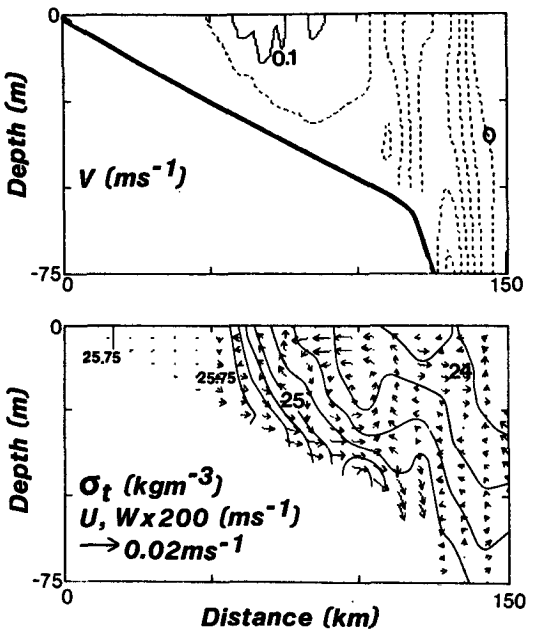

FIG. 12. Computed mean velocity and density fields at t = 55 days, 12 days after the third atmospheric forcing event has stopped. Arrows plotted as in Fig. 8.

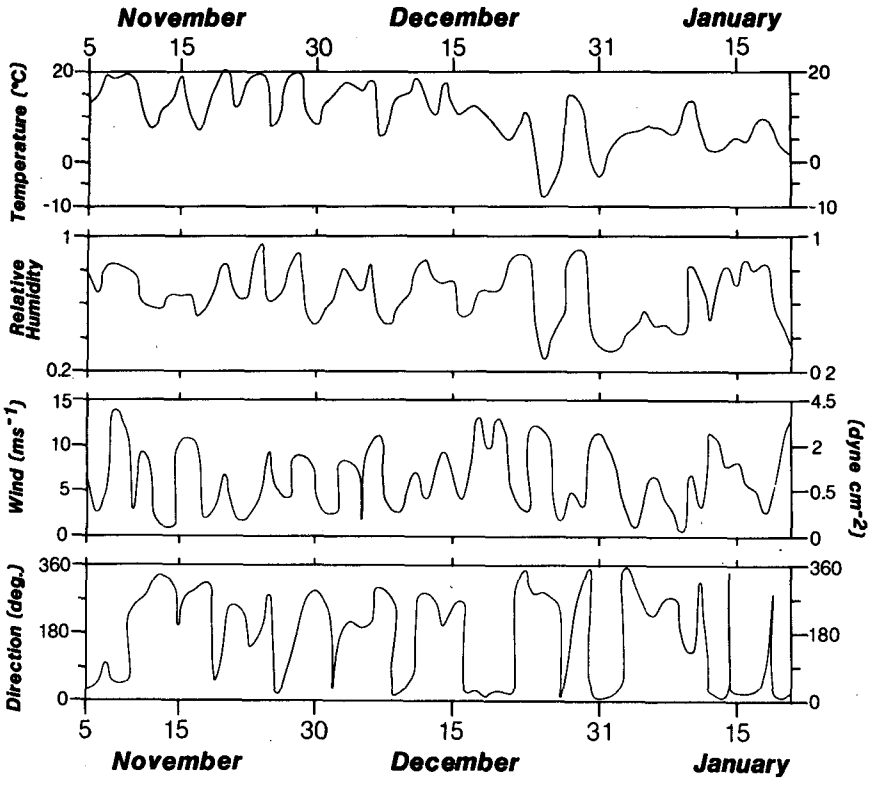

FIG. 13. Observed air temperature, relative humidity, wind speed and direction (from where wind blows, measured in degrees clockwise from true north) used as input forcing to model simulation from 5 November 1983 through 21 January 1984. The temperature and wind are from a navigational light tower located at the 17 m isobath about 20 km offshore of Savannah. Relative humidity is from NOAA local climatological data at Savannah airport.

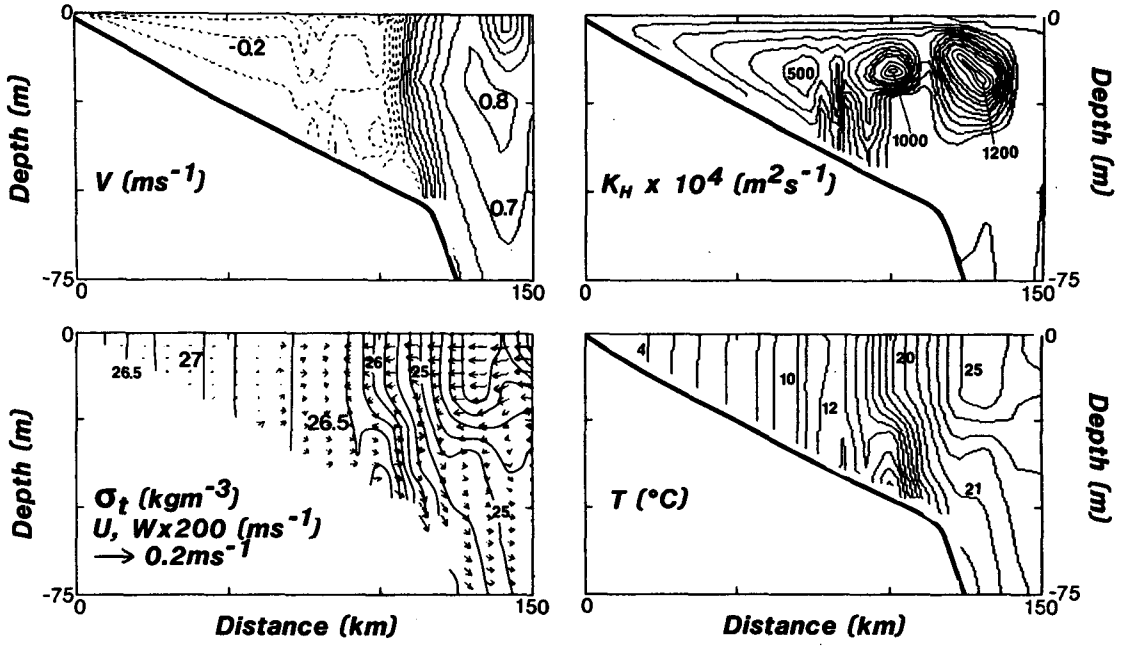

FIG. 14. Computed velocity, turbulence diffusivity, density and temperature fields on 21 January 1984. Model was forced using observed atmospheric data from 5 November 1983 through 21 January 1984. Arrows plotted as in Fig. 8.

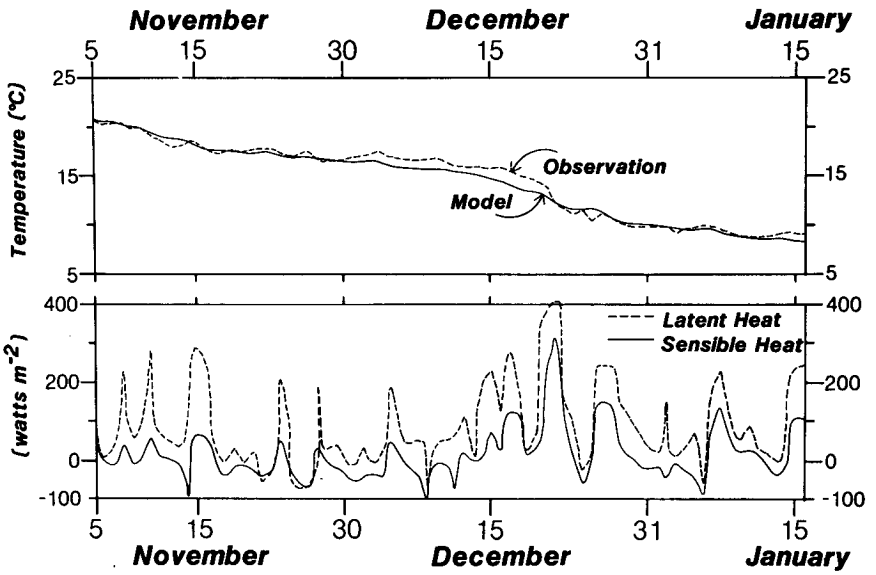

FIG. 15. Top panel: Comparison of observed and simulated temperature variation at 4 m below surface at a nearshore station (SNLT) situated on the 17 m isobath about 20 km offshore of Savannah; Bottom panel: Computed latent and sensible heat fluxes (upward flux positive) at SNLT.

convective overturning. Continental shelf water, inshore of about the 40 m isobath, shows diffused temperature (and density) structure with nearshore water reaching a low of 4°C. Other features of the response, including surface convergence and seaward near-bottom downwelling, are similar to those for the idealized atmospheric forcing case.

Comparison with Measured Temperature. Figure 15 compares computed and observed water temperatures at 14 m below the surface at SNLT. Also included in the figure are sensible and latent heat losses at SNLT. The agreement between model and observed temperature variations throughout the two and a half month period is fairly good. Both model and observations show fast temperature responses to CAOs signified by intense latent and sensible heat losses. One expects contributions to temperature variations from advective processes to be small at this nearshore station (SNLT). A one-dimensional (depth) version of the model was run and practically identical temperature variations, shown in Fig. 15, were obtained. The most serious discrepancy occurs between 1 and 18 December, which was an unusually warm period with small latent and sensible heat losses. The contribution to total sea-surface heat fluxes by incident solar radiation minus longwave back radiation should have been significant during this period and cannot be neglected in more realistic model simulations.

8. Discussion

Density fronts on the U.S. southeastern continental shelf during winter are formed by the combined actions of intrusions of warm upper Gulf Stream water and cooling of continental shelf water due to cycles of CAOs. Intrusion processes start with a breakdown of the shelf-break front due to: (i) onshore Ekman transport of upper Gulf Stream water due to strong southward winds and (ii) Gulf Stream meander and instability (Lee et al., 1981). Only the first case has been included in the present model study. Whatever their cause, Gulf Stream intrusions introduce warm water just inshore of the shelf break, ready to be flushed shoreward and mixed with cool continental shelf water by strong winter storms. Model results suggest that this shoreward intrusion of warm water occurs in a relatively short time (a few days) during a major winter storm. For the 1983/84 winter simulation, this occurred during storms in late December 1983 and in late January 1984. The front formed on the gently sloping continental shelf acts as a "barrier" separating warm outer shelf water from cooler inshore water. Despite winter cooling, outer shelf water is efficiently replaced by Gulf Stream water via cross-frontal circulation and should remain relatively warm. Inshore of the front, on the other hand, water is replaced only through small shoreward leakage across the front and seaward bottom flow at the foot of the front (Fig. 12). Therefore, inshore water dynamics and thermodynamics are approximately "local," and temperature and salinity variations are primarily determined by local exchange of heat and mass fluxes across the ocean surface. This explains why a one-dimensional (in depth) model adequately simulates temperature variations at an inshore ocean station (the SNLT). The situation is much different in

spring and summer when there is strong stratification and upwelling-favorable (northeastward alongshore) winds produce advective exchange between inshore and offshore waters (e.g., see Atkinson's, 1977, Fig. 1 and also Blanton and Atkinson, 1983, Fig. 8).

Adopting the sign convention that positive along-front direction has light water to the right, the continental shelf front, once formed, must be supported by a negative along-front wind stress. Otherwise, downwelling water accelerates seaward at the foot of the front and in time disperses the front. Model results suggest that this dispersion process takes more than ten days and, thus, there should be ample time for the next winter storm to arrive and strengthen the front. The wind induces downward turbulent diffusion of heat which balances the downwelling, seaward advection of cold water at the foot of the front. Thus, a vertical, strong front is maintained. The negative along-front wind stress also transports light surface water converging at the front, analogous to light estuarine water converging at a nearshore front as modeled by Csanady (1978) and observed by Blanton (1981) and Blanton and Atkinson (1983). However, the dynamics are different in the two cases. For an estuarine front, strong stratification prevents vertical turbulent mixing and a negative along-front wind stress would disperse the front.

Present model results suggest a northward mean flow of about 5 cm s^{-1} at middepth at the 30 m isobath (Fig. 12), about the same order as Lee's (1978) December 1976–April 1977 observations. These observations show northward mean velocities of about 6.5 and 2.5 cm s^{-1} for the two 30 m current meter moorings and about 10.6 cm s^{-1} for the 45 m mooring. Blanton's (1981, see his Fig. 11) results show that monthly mean sea level differences between Savannah, Georgia and Daytona Beach, Florida are small if averaged from December through April. The influence of this alongshore pressure gradient on the northward mean flow during winter is therefore somewhat uncertain. Perhaps the cross-shelf density contrast due to the continental shelf front explains part of the observed mean northward flow.

The Gulf Stream meander processes have been omitted in the present model study. These processes are clearly of utmost importance in studying the dynamics of breakdown of the shelf-break front and subsequent shoreward intrusion of upper Gulf Stream water. A proper study in this case would require a three-dimensional, time-dependent model. One would be interested, for example, in differentiating shoreward intrusion processes caused by Gulf Stream meanders from those caused by intense winter cyclones. Concurrent hydrographic and current meter measurements, coupled with satellite SST mappings, are necessary to achieve a more complete understanding of the dynamics and thermodynamics of the physical processes involved.

Acknowledgments. I wish to thank Susan Salyer for preparing the manuscript and Anna Boyette for drafting the figures. My thanks to D. Menzel, J. O. Blanton and Barbara Blanton for their critical reviews; to J. O. Blanton, L. P. Atkinson, J. M. Bane and T. N. Lee for helpful discussions, and to L. P. Atkinson, J. A. Yoder, J. O. Blanton and T. N. Lee for kindly allowing me to use their unpublished data.

APPENDIX

Implementation of Fine Grid–Coarse Grid System in a Numerical Finite-difference Model

The modification of an existing finite-difference model to allow for variable mesh feature is described here. This modeling feature is clearly useful in coastal circulation studies, for example, when one would like different model resolutions in different regions, but one perhaps cannot afford to spend a lot of effort in writing a new computer program. The method is as follows. Suppose we require fine-grid and coarse-grid regions with grid size ratios $\Delta x_c/\Delta x_f = \Delta y_c/\Delta y_f = 2$ (different ratios in x and y directions can be similarly treated) and let us consider the following two-dimensional advection equations for temperature (Fig. A1)

$$T_t + UT_x + VT_y = 0. \tag{A1}$$

As an example, a second-order accurate time and space difference equation is

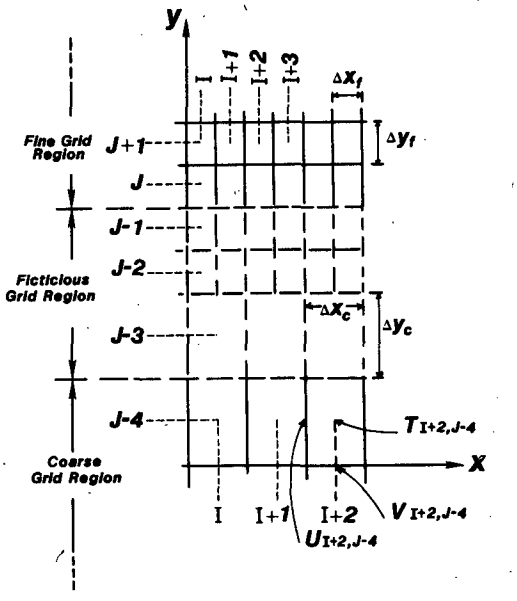

FIG. A1. Finite difference, fine grid–coarse grid matching configuration.

$$T_{i,j}^{n+1} = T_{i,j}^{n-1} - (\Delta t/\Delta x)[U_{i+1,j}(T_{i+1,j} + T_{i,j}) - U_{i,j}(T_{i,j} + T_{i-1,j})] - (\Delta t/\Delta y) \times [V_{i,j+1}(T_{i,j+1} + T_{i,j}) - V_{i,j}(T_{i,j} + T_{i,j-1})] \quad \text{(A2)}$$

in which grid variables without superscripts are understood to be at n time-level and the locations of U, V and T are defined in Fig. A1. Equation (A2) is valid both in the fine-grid and coarse-grid regions with (Δx, Δy) assigned appropriate values (Δx_f, Δy_f) or (Δx_c, Δy_c). It fails for the boundary rows across which (Δx, Δy) change values. In Fig. A1 this would occur for rows j-2 and j-3. To overcome this, three fictitious rows j-1, j-2 and j-3 are introduced and "meaningful" calculations actually start with row j increasing in the fine-grid region, and with row j-4 decreasing in the coarse-grid region. The fictitious rows are updated at every time step with a set of matching conditions. For example, T at grid $(i, j-3)$ in the coarse-grid region is updated with T at grids (i, j), $(i+1, j)$, $(i, j+1)$ and $(i+1, j+1)$ in the fine-grid region by simple averages. Other field variables can be similarly matched. Thus, the coarse-grid calculation "sees" the fine-grid calculation through row j-3, and the fine-grid calculation "sees" the coarse-grid calculation through rows j-1 and j-2. The need for two fictitious rows j-1 and j-2 in the fine-grid region stems from the staggered grid system and calculation of nonlinear advective term $[V^2(H+\eta)]_y$ for $V_{i,j}$, $V_{i+1,j}$, ..., etc., in the y-momentum equation. The method is easily extended to three-dimensional, especially when the vertical axis is expressed in sigma coordinate $\sigma = (z-\eta)/(H+\eta)$.

Recently, Mellor and Galperin (private communication, 1985) improved the method by matching "fluxes," instead of grid point values, and have reported some success in their work on Delaware River estuary–continental shelf modeling.

REFERENCES

Atkinson, L. P., 1977: Modes of Gulf Stream intrusion into the South Atlantic Bight shelf waters. *Geophys. Res. Lett.*, **4**, 583–586.

Blanton, J. O., 1981: Ocean currents along a nearshore frontal zone on the continental shelf of the southeastern United States. *J. Phys. Oceanogr.*, **11**, 1627–1637.

——, and L. P. Atkinson, 1983: Transport and fate of river discharge on the continental shelf of the southeastern United States. *J. Geophys. Res.*, **88**, 4730–4738.

Blumberg, A. F., and G. L. Mellor, 1983: Diagnostic and prognostic numerical circulation studies of the South Atlantic Bight. *J. Geophys. Res.*, **88**, 4579–4592.

Brooks, D. A., and J. M. Bane, Jr., 1983: Gulf Stream meanders off North Carolina during winter and summer 1979. *J. Geophys. Res.*, **88**, 4633–4650.

Bumpus, D. F., 1973: A description of the circulation on the continental shelf of the east coast of the United States. *Progress in Oceanography*, Vol. 6, Pergamon, 111–156.

Csanady, G. T., 1978: Wind effects on surface to bottom fronts. *J. Geophys. Res.*, **83**, 4633–4640.

Dickey, T. D., and J. C. Van Leer, 1984: Observations and simulation of a bottom Ekman layer on a continental shelf. *J. Geophys. Res.*, **89**, 1983–1988.

Fofonoff, N. P., 1962: Physical properties of sea-water, in *The Sea*, Vol. 1, M. N. Hill, Ed., Interscience, 3–30.

Garwood, R. W., R. Fett, K. Rabe and H. Brandli, 1981: Ocean frontal formation due to shallow water cooling effects as observed by satellite and simulated by a numerical model. *J. Geophys. Res.*, **86**, 11000–11012.

Gill, A. E., 1982: *Atmospheric-Ocean Dynamics.* Academic Press, 662 pp.

Hassid, S., and B. Galperin, 1983: A turbulence energy model for geophysical flows. *Bound. Layer Meteor.*, **26**, 397–412.

——, and ——, 1984: A turbulent energy model for diffusion in the convective boundary layer. *Atmos. Environ.*, **18**, 1081–1089.

Huh, O. K., W. J. Wiseman, Jr. and L. J. Rouse, Jr., 1978: Winter cycle of sea surface thermal patterns, northeastern Gulf of Mexico. *J. Geophys. Res.*, **83**, 4523–4529.

——, L. J. Rouse, Jr. and N. D. Walker, 1984: Cold air outbreaks over the northwest Florida continental shelf: Heat flux processes and hydrographic changes. *J. Geophys. Res.*, **89**, 717–726.

Kantha, L. H., A. F. Blumberg, H. J. Herring and G. L. Mellor, 1981: The physical oceanographic and sea surface flux climatology of the South Atlantic Bight. Rep. 70, Dynalysis of Princeton, Princeton, NJ, 52 pp.

Lee, T. N., 1978: Measurement of Gulf Stream and wind induced shelf circulation in the South Atlantic Bight. University of Miami Prog. Rep. to DOE, Contract EY-76-S-05-5163, 73 pp.

——, L. P. Atkinson and R. Legeckis, 1981: Observations of a Gulf Stream frontal eddy on the Georgia continental shelf, April 1977. *Deep Sea Res.*, **28**(A), 347–378.

Martin, P. J., 1985: Simulation of the mixed layer at OWS November and Papa with several models. *J. Geophys. Res.*, **90**, 903–916.

Mellor, G. L., and T. Yamada, 1982: Development of a turbulence closure model for geophysical fluid problems. *Rev. Geophys. Space Phys.*, **20**, 851–875.

Nowlin, W. D., and C. A. Parker, 1974: Effects of a cold-air outbreak on shelf waters of the Gulf of Mexico. *J. Phys. Oceanogr.*, **4**, 467–486.

Oey, L.-Y., G. L. Mellor and R. I. Hires, 1985a: A three-dimensional simulation of the Hudson-Raritan estuary. Part I: Description of the model and model simulations. *J. Phys. Oceanogr.*, **15**, 1676–1692.

——, —— and ——, 1985b: A three-dimensional simulation of the Hudson-Raritan estuary. Part II: Comparison with observation. *J. Phys. Oceanogr.*, **15**, 1693–1709.

——, —— and ——, 1985c: A three-dimensional simulation of the Hudson-Raritan estuary. Part III: Salt flux analyses. *J. Phys. Oceanogr.*, **15**, 1711–1720.

Roll, H. U., 1965: *Physics of the Marine Atmosphere.* Academic Press, 426 pp.

Wang, D.-P., 1984: Mutual intrusion of gravity current and density front formation. *J. Phys. Oceanogr.*, **14**, 1191–1199.

Weber, A. H., and J. O. Blanton, 1980: Monthly mean wind fields for the South Atlantic Bight. *J. Phys. Oceanogr.*, **10**, 1256–1263.